Current and Future Applications of 3-D Global Earth-Ionosphere Waveguide Models Based on the Full-Vector Maxwell's Equations FDTD Method

Jamesina J. Simpson

Assistant Professor, Electrical and Computer Engineering Department

MSC01 1100, 1 University of New Mexico, Albuquerque, NM, 87131, USA

Email: simpson@ece.unm.edu

***Abstract* —** Advances in computing technologies in recent decades have provided a means of generating and performing highly sophisticated computational simulations of electromagnetic phenomena. In particular, just after the turn of the 21st century, improvements to computing infrastructures provided for the first time the opportunity to conduct advanced, high-resolution three-dimensional full-vector Maxwell's equations investigations of electromagnetic propagation throughout the global Earth-ionosphere spherical volume. In particular, global models employing the finite-difference time-domain (FDTD) method are capable of including such details as the Earth's topography and bathymetry, as well as arbitrary horizontal / vertical geometrical and electrical inhomogeneities and anisotropies of the ionosphere, lithosphere, and oceans. Studies at this level of detail simply are not achievable using analytical methods. The goal of this Paper is to provide an historical overview and future prospectus of global FDTD computational research for both natural and man-made electromagnetic phenomena around the world. Current and future applications of global FDTD models relating to lightning sources and

UU IR Author Manuscript

radiation, Schumann resonances, hypothesized earthquake precursors, remote sensing, and space weather are discussed.

Keywords — Finite-Difference Time-Domain (FDTD) method, Earth, ionosphere, plasma, waveguide, propagation, lightning, sprites, whistlers, ionospheric disturbances, remote-sensing, oil field, earthquake precursor, coronal mass ejection, Schumann resonance.

UU IR Author Manuscript

I. INTRODUCTION

Advances in computing technologies in recent decades have provided a means of generating and performing highly sophisticated computational simulations of electromagnetic (EM) phenomena. In particular, just before the turn of the 21st century, improvements to computing infrastructures provided for the first time the opportunity to conduct advanced, high-resolution three-dimensional (3-D) full-vector Maxwell's equations investigations of EM propagation throughout the global Earth-ionosphere spherical volume [Simpson 2007]. Employing the finite-difference time-domain (FDTD) method [Yee 1966, Taflove and Hagness 2005], these numerical models are capable of including such details as the Earth's topography and bathymetry, as well as arbitrary horizontal / vertical geometrical and electrical inhomogeneities and anisotropies of the ionosphere, lithosphere, and oceans.

The goal of this Paper is to provide an historical overview and future prospectus of global FDTD computational research for EM propagation around the world. Earth-ionosphere models employing FDTD pose significant advantages over any other current or previous analytical / computational methodologies. In addition to solving the full-vector Maxwell's equations, FDTD simulations may accommodate not only complex geometries and anisotropies, but they also inherently calculate the time-marching behavior of impulsive EM phenomena throughout those very complex environments. This permits single-run calculations of *both* transient and steady-state solutions over spectral ranges of interest via a discrete Fourier Transform.

Indeed, the primary limitations of global FDTD Earth-ionosphere waveguide modeling is not so much in the computational technique itself, or in the availability of massively parallel / advanced computational resources to run the FDTD simulations. Instead, the primary limitations may be considered the availability of detailed / high-resolution ionospheric and lithospheric data,

as well as complete knowledge of many source characteristics (such as for sources induced from stresses in the Earth's crust as detailed in Section III(B) or for space weather-induced ionospheric currents as described in Section IV(C)). But, as further scientific advances are made through improved measurements and analyses, the computational means of including in FDTD models many of these details and their effects is already possible.

FDTD was first proposed in [Yee 1966] and later named in [Taflove 1980]. Over the past three decades, the popularity and utility of the FDTD method for EM propagation and interaction modeling has increased substantially. Sevgi, Akleman, and Felsen [2002] "trace the development of methodologies from the early, idealized, analytically tractable modeling [of wave propagation] to successively more realistic approaches, made possible by the availability of massive computational resources." They begin with analytical ray and mode techniques, progress to a frequency-domain algorithm, and finish with their more recent FDTD-based wave propagator for signals above 1 MHz. Sevgi, Akleman, and Felsen conclude that the FDTD-based algorithm is "efficient and reliable for broadband (pulse) propagation," and that although FDTD can be computationally expensive, "the need for physics-based numerical algorithms is likely to continue." Indeed, Cummer similarly concludes in [Cummer 2000] regarding two-dimensional (2-D) FDTD modeling of long-range propagation that "the simplicity of FDTD propagation modeling and ever-increasing computer power probably make FDTD the technique of the future."

Considering that there are good prospects for ongoing improvements to computing technologies, the future utility and employment of advanced 3-D FDTD models of the complex global Earth-ionosphere waveguide is especially bright. Already, to date, global FDTD simulations below about 1 kHz have been conducted for studies of wave propagation involving

complex interactions with the lithosphere, oceans, and ionosphere that lead to resonances literally involving the entire Earth-ionosphere cavity. Applications of this work have included Schumann resonances, hypothesized earthquake precursors, and remote sensing of ionospheric disturbances and oil fields (see [Simpson and Taflove 2007] and references therein).

But, as computing capabilities continue to improve over time, the resolution and radial extent of FDTD Earth-ionosphere models may correspondingly increase. The standard FDTD algorithm requires about 10 - 20 grid cells per wavelength [Taflove and Hagness 2005], so as the grid resolution increases, higher frequency and thus also higher altitude numerical investigations may be conducted. This will open up entirely new areas of investigations on a global scale, such as global lightning occurrences and rates (which to date have only been modeled on a local level, as discussed in Section II(B)), anisotropic wave propagation introduced by the global Earth's geomagnetic field and ionosphere plasma, and a variety of space weather effects on the ionosphere and ground-level electric and magnetic fields.

This Paper is organized to first provide an historical review of FDTD developments that led to the first generations of fully 3-D global FDTD models of the Earth-ionosphere waveguide. Section II steps through the original 2-D FDTD models and their applications, then follows with a description of the first fully 3-D global FDTD models developed independently by [Hayakawa and Otsuyama 2002, Otsuyama and Hayakawa 2004] and [Simpson and Taflove 2004a, Simpson et al. 2006].

Next, Section III of this Paper describes applications published to date of the 3-D global FDTD models of the Earth-ionosphere spherical volume. An organized list of the principle previously published 2-D and 3-D FDTD Earth-ionosphere waveguide modeling techniques and their corresponding applications (as covered in Sections II and III) is provided in Table 1.

Then, Section IV examines ongoing and future possibilities / utility of the global 3-D FDTD models that may come about as computing technologies continue to improve in the coming years and decades. Finally, Section V concludes the Paper.

Principal Techniques	Notable Features (to date)	Applications (to date)
2-D great circle cut propagation models [Berenger 1994a, Thevenot et al. 1999, Berenger 2002a, Berenger 2002b, Berenger 2005]	Ionosphere anisotropy [Thevenot et al. 1999]; surface-impedance ground boundary [Berenger 1994a]; isotropic geomagnetic field [Thevenot et al. 1999]; gyrotropic (anisotropic) ionosphere [Berenger 2002a]; numerical dispersion compensation [Berenger 2002a]; moving computational spatial domain [Thevenot et al. 1999]; numerical anisotropy removal [Berenger 2005]	Long-distance propagation modeling [Berenger 1994a, Thevenot et al. 1999, Berenger 2002a, Berenger 2002b, Berenger 2005]; nuclear burst [Berenger 2002b]
2-D azimuthally symmetric models of the local Earth-ionosphere waveguide surrounding a source [Cummer 2000, Hu and Cummer 2006, Hu et al. 2007, Yang and Zhou 2004, Poussard and Corcuff 2000, Otsuyama and Hayakawa 2002, Kuo et al. 2007]	Cold plasma ionosphere [Cummer 1997 and references therein]; Magnetized cold plasma ionosphere [Hu and Cummer 2006]; Nearly perfectly matched layer boundary conditions for the plasma ionosphere [Cummer 2003]; Earth curvature correction [Hu and Cummer 2006]; surface-impedance ground boundary [Hu and Cummer 2006]; coupling with an electron density continuity equation [Kuo et al. 2007]	Propagation from lightning [Cummer 2000, Hu and Cummer 2006, Yang and Zhou 2004]; trimpis (whistlers, sprites, elves) [Hu et al. 2007, Poussard and Corcuff 2000, Otsuyama and Hayakawa 2002, Kuo et al. 2007]
3-D azimuthally symmetric models of the entire Earth-ionosphere waveguide [Soriano et al. 2005, Yang and Pasko 2005, Navarro et al. 2008]; and of other planetary	Azimuthally-averaged International Reference Ionosphere (IRI) model to derive an effective ionosphere conductivity profile [Navarro et al. 2008]	Schumann resonances [Soriano et al. 2005, Yang and Pasko 2005, Navarro et al. 2008]; x-ray bursts and solar proton events [Yang and Pasko 2005, Navarro et al.

bodies [Yang et al. 2006, Soriano et al. 2007]		2008]; Schumann resonances on other planetary bodies [Yang et al. 2006, Soriano et al. 2007]
Fully 3-D latitude-longitude models of the entire Earth-ionosphere waveguide [Hayakawa and Otsuyama 2002, Otsuyama and Hayakawa 2004, Simpson and Taflove 2004a, Simpson and Taflove 2005a, Simpson and Taflove 2005b, Simpson 2008, Yang and Pasko 2006, Yang and Pasko 2007, Yang et al. 2009, Ando et al. 2005]	Entire-Earth topography [Simpson and Taflove 2004a]; spatially variable conductivity of the lithosphere, oceans, and ionosphere [Simpson and Taflove 2004a]; IRI model [Yang and Pasko 2006]; polar region cell-combining technique [Simpson and Taflove 2004a]; variable grid resolution in the vertical (radial) direction [Simpson and Taflove 2005b]	Propagation [Hayakawa and Otsuyama 2002, Otsuyama and Hayakawa 2004], Simpson and Taflove 2004a]; oil field radar [Simpson and Taflove 2005b]; preseismic lithospheric current sources [Simpson and Taflove 2005a, Simpson 2008]; Schumann resonances [Ando et al. 2005, Yang and Pasko 2006, Yang and Pasko 2007, Yang et al. 2009];
Fully 3-D geodesic models of the entire Earth-ionosphere waveguide [Simpson et al. 2006, Simpson and Taflove 2006]	Entire-Earth topography [Simpson et al. 2006]; spatially variable conductivity of the lithosphere, oceans, and ionosphere [Simpson et al. 2006]; variable grid resolution in the vertical (radial) direction [Simpson et al. 2006]	Propagation [Simpson et al 2006]; radar for ionospheric anomalies [Simpson and Taflove 2006]; oil field radar [Simpson et al. 2006];

Table 1. Summary of principal techniques and applications for FDTD computational modeling of electromagnetic wave propagation in the Earth-ionosphere waveguide (adapted and updated from [Simpson and Taflove 2007]).

II. A HISTORICAL SKETCH OF THE DEVELOPMENT OF 3-D GLOBAL EARTH-IONOSPHERE FDTD MODELS

A. LONG-RANGE 2-D PROPAGATION MODELING

Berenger was the first to use the FDTD method to model subionospheric wave propagation at frequencies below 300 kHz. His conference abstracts in this area date back to 1994 [Berenger

1994a]. His work had two initial goals: (1) to compare FDTD results with previous frequency-domain mode theory calculations [Pappert and Ferguson 1986]; and (2) to create an entirely new model having the capability of accommodating continuously varying parameters over the propagation path.

The basis for Berenger's first model is a 2-D Cartesian-coordinate grid extending from the Earth's surface upwards to the effective reflection height in the ionosphere at the frequency of interest, and extending a few thousand kilometers (km) laterally along a great-circle cut. Perfect electric conductor (PEC) boundary conditions terminate the grid on all sides of the computational domain, and a surface impedance boundary condition is applied at the Earth's surface to model the finite conductivity of the lithosphere or ocean. Initially the geomagnetic field is not taken into account. However it is later modeled in [Thevenot et al. 1999] by way of solving the differential equations governing the current density in the ionosphere. Then the formulation of [Berenger 2002a] achieves a gyrotropic (anisotropic) ionosphere model, a feature particularly important for nighttime propagation.

In [Thevenot et al. 1999, Berenger 2002a, Berenger 2002b], several techniques are developed to reduce the computational burden of modeling propagation over several megameters (Mm). For example, [Thevenot et al. 1999] introduces a technique involving a moving computational spatial domain extending backwards from the wavefront until steady state is attained. So long as reflections from the rear grid edge (opposite to the direction of interest) and propagation speeds are carefully considered, this technique can be used to significantly decrease the size of the grid.

A second way the computational burden is reduced is by counteracting the numerical angular dispersion inherent to the FDTD mesh [Berenger 2002a]. This strategy permits the use

of coarser grids. That is, high-resolution meshes are needed for subionospheric propagation in the 3 – 300 kHz range because "more than ten modes contribute significantly to the field strength" [Berenger 2002a]. Each of these modes propagates with a different eigenangle, and therefore accrues a different phase shift at varying distances from the source. This issue is addressed in [Berenger 2002a] by introducing an anisotropic permeability. Specifically, an artificial (for better numerical results) permeability μ_r is incorporated into the radial (vertical) derivatives of Maxwell's equations [Berenger 2002a, Berenger 2002b]. This technique provides very good results for propagation at a single frequency or over a narrow range of frequencies, and for propagating modes having eigenangles within a certain range.

In his work, Berenger shows good agreement between waveguide mode theory and FDTD calculations for single-frequency propagation from a vertical dipole antenna. He considers typical daytime and nighttime ionosphere conductivity profiles, transitions between day and night, and disturbed conditions during a nuclear burst [Thevenot et al. 1999, Berenger 2002b]. Berenger finds that FDTD is more computationally demanding than mode theory, but he notes that ongoing improvements in computer resources will continue to decrease simulation times in the future. Further, he states that FDTD "is more versatile than the waveguide method" since it can provide results for general wideband and impulsive applications [Berenger 2002b].

B. 2-D MODELING OF LIGHTNING SOURCES AND RADIATION

In addition to long-range propagation modeling, 2-D FDTD propagation models have also been applied to the area of lightning, the strongest natural source of waves in the 3 Hz – 30 kHz frequency range at the Earth's surface. Cummer [2000] compares 2-D FDTD results to mode theory and analytical calculations for propagation in this frequency band from a broadband

lightning discharge over a 1000-km lossy ground path. For this study, he employs a cylindrical-coordinate FDTD grid having a PEC ground and an anisotropic but frequency-independent conducting ionosphere (assumes the collision frequency is much higher than the wave frequency at all altitudes).

Reference [Cummer 2000] reports "extremely good" agreement between numerical mode theory and FDTD for nighttime spectra below 10 kHz radiated from the lightning source, and a comparable level of agreement for the daytime spectra. In [Cummer 2000], Cummer also finds that a "major strength of the FDTD technique… is that all of the fields (discharge and post-discharge, evanescent and propagating) are automatically calculated, while most other solution techniques are forced to treat these fields separately."[1] The evanescent fields become increasingly important at lower frequencies and shorter distances from a lightning stroke. Further, FDTD can, in principle, permit straightforward modeling (with no increase in simulation time) of arbitrary horizontal as well as vertical inhomogeneities of the atmosphere and Earth.

Later, in [Hu and Cummer 2006], the 2-D cylindrical FDTD model described in [Cummer 2000] is advanced by treating the ionosphere as a magnetized cold plasma (see [Cummer 1997] and references therein for a description of previous non-magnetized cold plasma algorithms). Their new model includes the effects of charged particles (electrons, positive ions, and negative ions). It also includes an Earth's curvature correction, as well as a surface impedance boundary condition (SIBC) [Maloney and Smith 1992, Kellali et al. 1993] for modeling the lossy ground. As a result, the model of [Hu and Cummer 2006] provides improved accuracy to altitudes of up to ~200 km and frequencies up to ~ 30 kHz. The model of [Hu and Cummer 2006] is validated by comparing FDTD calculations to mode theory solutions and broadband experimental data.

[1] **Note that these claims are strictly speaking applicable only to equivalent wavelengths that are adequately resolved by the FDTD grid.**

Fig. 1 (courtesy of [Hu and Cummer 2006]) compares the FDTD model results with experimental data for the frequency spectra of ten sferics radiated from negative lightning discharges at distances of about 629 km. These ten sferics are accurately aligned in the time-domain and averaged to improve the signal-to-noise-ratio. The level of agreement is "very strong" considering the number of uncertainties that prevent a better comparison [Hu and Cummer 2006].

In [Yang and Zhou 2004], a 2-D cylindrical coordinate FDTD model is also employed to study EM fields very close to lightning channels. The calculated vertical electric (*E*)-field is shown to agree with measurements taken at 15 m distance. Further, the horizontal *E*-field at a distance of 100 m agrees with the Cooray-Rubinstein approximation [Cooray 1992, Rubinstein 1996].

Lightning discharges have been associated with complicated phenomena in the lower ionosphere that result in Trimpis, or transient perturbations (amplitude and phase) of subionospheric signals [Strangeways 1996]. Two classes of Trimpis exist, both of which have been studied using FDTD, among other methods. The first class is known variously as lightning-induced electron precipitation (LEP) Trimpis, classic Trimpis, or whistler-induced electron precipitation (WEP) Trimpis. The second class, known as early Trimpis or early/fast Trimpis, are those assumed not caused by lightning-induced electron precipitation because of their very short onset delay after a lightning discharge. Instead, they are caused by a direct heating of the ionosphere by the lightning. This second class includes sprites and elves.

In [Poussard and Corcuff 2000], the first class of Trimpis is studied using the FDTD method. A 2-D FDTD model based on Berenger's initial propagation code [Berenger 1994a] is employed. However, the model of [Poussard and Corcuff 2000] includes all six field

components and no phase information. As a result, Poussard and Corcuff propose a hybrid system involving both FDTD and mode theory to study propagation below 10 kHz, and predict the location, longitudinal extent, and height of disturbed regions associated with the Trimpi events. Their results show good agreement with temporal signatures measured in France for signals arriving from England and the United States.

In [Otsuyama and Hayakawa 2002], the second class of Trimpis are studied using the FDTD method. They employ a 2-D FDTD model of a 500-km-long propagation path bounded by a PEC Earth and an ionosphere having an exponential conductivity profile. They first calculate scattering from sprite-induced plasma sheets of varying widths and distances and extending 20 km downwards from the ionosphere. Second, they calculate EM scattering from ionospheric perturbations associated with elves extending 10 km downwards from the ionosphere. These perturbations are assumed to be regions of increased ionization expanding outwards (radially) for 1.5 msec to a total of 450 km, followed by a decay of ionization expanding outwards at the same rate and over the same region. Results in [Otsuyama and Hayakawa 2002] show that scattering at 40 kHz by elves is significantly larger than those from sprites. In fact, the calculated scattering from sprites is so small the authors hypothesize that a weak perturbed region in the ionosphere extending laterally beyond the approximately 40-km-diameter sprite (as observed by optical measurements) must exist.

In [Kuo et al. 2007], FDTD is utilized to model the emissions between 185 and 800 nm of elves and their spatial-temporal evolutions. A cylindrical-coordinate grid is generated that solves the Maxwell's equations coupled with an electron density continuity equation. It extends to an altitude of 100 km, and over a range of 600 km; a PEC ground is assumed. Three major atmospheric attenuation mechanisms are considered: O_2, O_3, and molecular Rayleigh scattering.

Very good agreement is obtained between the calculated and observed photon fluxes in the ISUAL spectrophotometric channels on the FORMOSAT-2 satellite and between the simulated and observed morphologies of elves.

In [Hu et al. 2007], a 2-D cylindrically symmetric FDTD model is utilized to simulate lightning-generated electromagnetic fields. Hu et al. compare simulated mesospheric electric fields to threshold electric field for conventional breakdown to test whether conventional breakdown (thus a sprite) would be initiated and at what altitude. They compare measurements and theory with their FDTD results for sprites having both short and long delays from the source lightning strikes.

Finally, specific FDTD techniques have been published for modeling wave generation by lightning. For example, [Sarto 2001] presents an absorbing boundary condition specifically for where / when the space-cell size is several thousand times smaller than the minimum wavelength, such as for the case of lightning interaction with complex structures. Second, Berenger introduces in [2005] a post-processing technique for removing most of the numerical anisotropy of the FDTD mesh when modeling propagation over large distances (> 5000 km), thereby allowing coarser grids to be used. (His previous single-frequency correction technique of [Thevenot et al. 1999] is not applicable to studies involving broadband lightning.) Berenger finds that the time required for post-processing is significantly less than the computational costs of using a finer mesh.

A third FDTD technique that has been developed for modeling local wave propagation from lightning is the nearly perfectly matched layer (NPML) [Cummer 2003]. NPML was originally developed to ease the implementation of the perfectly matched layer (PML) boundary condition

[Berenger 1994b, Taflove and Hagness 2005] in an ionospheric cold plasma. However, NPML was later shown by Berenger to be a true PML [Berenger 2004].

C. THE FIRST FULLY 3-D GLOBAL FDTD MODELS OF THE EARTH-IONOSPHERE WAVEGUIDE

Two groups independently published the first fully 3-D global FDTD models of the Earth-ionosphere waveguide. One group, in [Hayakwa and Otsuyama 2002, Otsuyama and Hayakawa 2004], reports a spherical-coordinate, latitude-longitude model of the Earth-ionosphere waveguide based upon fundamental work in [Holland 1983]. Their grid resolution is 250 x 250 x 2 km, and they assume a PEC ground and typical exponential conductivity profiles for the ionosphere according to [Holland 1983]. Because they use the same grid as Holland, their model is subject to increasing space-cell eccentricity upon approaching the poles due to converging meridians.

In [Hayakwa and Otsuyama 2002, Otsuyama and Hayakawa 2004] a lightning discharge is simulated at the equator having a double-exponential current time-waveform similar to that reported by Bruce and Golde [1941]. The calculated radiated waveforms and wave impedances are compared at several distances (between 5 and 20 Mm) from the source to those predicted by previous analytical formulations [Nickolaenko at al. 1999, Nickolaenko and Hayakawa 1998]. Further, the effect of modeling one-half of the Earth having a daytime ionosphere profile and the other half having a nighttime profile is investigated for both the symmetrical and more realistic tilted cases (relative to the Sun) with respect to the North and South Poles [Otsuyama and Hayakawa 2004].

The second group, in [Simpson and Taflove 2002, Simpson and Talove 2004a, Taflove and Simpson 2005], reports a global latitude-longitude spherical-coordinate FDTD model of the Earth-ionosphere waveguide also based upon fundamental work in [Holland 1983]. However, their model includes a means to reduce the eccentricity of the cells in the polar regions by a novel adaptive cell-combining technique applied to adjacent grid-cells in the East-West direction. This technique permits maintenance of the time-step at nearly the level allowed by the Courant stability condition for the square equatorial cells, yielding a greatly improved computational efficiency relative to conventional spherical-coordinate formulations.

Initially working towards a 3-D model, Simpson and Taflove begin with a 2-D spherical-coordinate, transverse magnetic (TM) grid of the Earth's surface [Simpson and Taflove 2002]. Fig. 2 illustrates the layout of the TM latitude-longitude FDTD model as seen from a constant radial coordinate. This model is employed to track an impulsive circular wave as it propagates radially outward from a filamentary current source having a Gaussian time-waveform. The radiated pulse travels completely around the Earth-sphere model and then propagates radially inward towards the antipode. Results are shown in [Simpson and Taflove 2002] for a lossless 1024×512 grid spanning the Earth-sphere. A high degree of numerical isotropy is demonstrated for numerical wave propagation within the model despite concurrent wave propagation through both simple, uniform grid regions near the equator and more complicated polar regions having a nonuniform mesh. Further, the 180° phase reversals of the *E*-field at the antipode first calculated in [Wait 1965] is demonstrated, as well as a fundamental Earth-ionosphere-cavity resonance of 7.46 Hz.

In [Simpson and Taflove 2004a], Simpson and Taflove expand the 2-D work of [Simpson and Taflove 2002] to create a fully 3-D FDTD model of the entire Earth-ionosphere cavity

extending between ±100 km of sea level. Their 3-D space lattice has a nominal resolution of 40 x 40 x 5 km at the equator, and allows for variable cell size in the radial (vertical) direction. The East and West sides of the grid are connected to permit uninterrupted EM wave propagation around the Earth in the equatorial direction. Only a single-processor laboratory computer with 2 GB of memory is needed to process the model, however simulation times may be reduced from days / weeks to hours using a cluster of processors and a parallelized model. Further, higher resolutions may be achieved with a parallelized code.

For the 3-D latitude-longitude model of [Simpson and Taflove 2004a], Simpson and Taflove use topographic and bathymetric data from the NOAA-NGDC "Global Relief CD-ROM." Lithosphere conductivity is then assigned according to Fig. 3 [Hermance 1995], depending upon whether the space lattice point is located directly below an ocean or within a continent. Isotropic ionospheric conductivity is assigned according to the exponential profile used in [Bannister 1985], which permits (for validation purposes) the most straightforward comparison of the present FDTD modeling results with the data reported in [Bannister 1984], since EM propagation is crucially affected by the characteristics of the ionosphere. However, Simpson and Taflove [2004a] note that FDTD models are capable of significantly greater ionospheric detail, i.e. day-to-night transitions, anisotropy, geomagnetic effects, etc., than that possible using the analysis of [Bannister 1984] or other analytical methods.

To first validate their 3-D model, Simpson and Taflove excite the grid just off the equator at 47° W with a vertical, 5-km-long current pulse having a Gaussian time-waveform. Fig. 4 (courtesy of [Taflove and Simpson 2005]) shows snapshots of the globally propagating impulsive EM wave radiated from the current pulse as calculated by their 3-D FDTD model.

The FDTD propagation modeling results are found to be accurate to ±1 dB over the range 50–500 Hz relative to the results of [Bannister 1984].

Simpson and Taflove, in collaboration with climatologist R. Heikes, have also developed an alternative 3-D geodesic grid [Randall et al. 2002] of the global Earth-ionosphere cavity extending between ±100 km of sea level [Simpson et al. 2006]. As for the Simpson-Taflove latitude-longitude grid, they initially begin with a 2-D spherical-coordinate, TM geodesic grid of the Earth's surface [Simpson and Taflove 2004b, Taflove and Simpson 2005]. This model employs hexagonal grid cells with a small, fixed number of pentagonal grid cells to span the spherical surface at each radial coordinate. Fig. 5 (a) illustrates the layout of the TM geodesic FDTD model as seen from a constant radial coordinate. Note in Fig. 5 (b) that the grid may be divided into five or more equal panels in a straightforward manner for ease of parallelization on a supercomputer.

In [Simpson et al. 2006], the 2-D geodesic model is extended to a fully 3-D FDTD geodesic grid allowing for variable cell size in the radial direction, and including details of the Earth's topography, bathymetry, and lithosphere and atmosphere conductivity values at a resolution of ~63 x 63 x 5 km. This model is validated in the same manner as the latitude-longitude 3-D grid described above and in [Simpson and Taflove 2004a]. The propagation modeling results are found to be accurate to within about ±0.5 dB/Mm in the frequency range of 50 – 500 Hz relative to the results of [Bannister 1984].

The geodesic grid of [Simpson et al. 2006] is superior to the previously reported Simpson-Taflove latitude-longitude grid of [Simpson and Taflove 2004a] in a number of respects. First, the geodesic grid completely avoids grid-cell convergences at the North and South Poles. Therefore, it provides much more numerically isotropic wave propagation and is simpler to

construct. Second, the geodesic grid ports readily and efficiently to a massively parallel supercomputer. Third, it permits an easier interchange of data with state-of-the-art Earth-simulation codes used by the geophysics community.

III. PREVIOUS APPLICATIONS OF 3-D GLOBAL FDTD MODELS

A. SCHUMANN RESONANCES

In 1952, W. O. Schumann predicted the resonant frequencies of the Earth-ionosphere cavity below about 100 Hz, which are now called Schumann resonances (SR) [Schumann 1952]. Interest in SRs have increased in recent years because of the apparent correlation between the resonant frequencies and global temperature changes [Williams 1992], as well as with global lightning activity [Williams 2005]. Further, SRs can be studied on other planetary bodies to provide information about their ionospheres [Pechony and Price 2004]. To date, FDTD studies of SRs have been conducted by three groups, as described in the following text.

The first group, in [Ando et al. 2005], uses the global 3-D model described in [Hayakawa and Otsuyama 2002, Otsuyama and Hayakawa 2004] and in Section II(C) to perform FDTD SR calculations. Ando et al. [2005] simulate a lightning strike occurring at the equator and record the E and magnetic (H) fields at distances between 5 and 20 Mm. Their results show that the amplitude and width of the SR peaks strongly depend on the source-observer distance. Further, they find that the FDTD-calculated SR peaks for the first and second modes are consistent with previous analytical calculations [Nickolaenko and Hayakawa 2002, Sentman 1995].

The second group, in [Soriano et al. 2005], uses an azimuthally-symmetric 3-D spherical-coordinate FDTD model to conduct SR studies. Their model resolution is 1.5° laterally and 5 km vertically, and they assume a PEC ground. First, a lossless Earth-ionosphere cavity is

considered, with a PEC ionosphere boundary at a height of 60 km. Good agreement is obtained between the FDTD-calculated resonances and previous analytical and transmission line matrix (TLM) results [Morente et al. 2003]. However, because their calculated results differ from actual measurements, Soriano et al. progress to a more advanced model including losses in the ionosphere. Soriano et al. model the quiet-ionosphere conductivity profiles of [Morente et al. 2003] and [Schlegel and Fuellekrug 1999] to a height of 100 km. The results obtained using this improved ionosphere model are in much better agreement with those of a semi-analytical two-scale height ionosphere model [Sentman 1990] and with actual measurements. For example, the FDTD deviations from experimental results using the improved ionosphere model range from 3% for the third mode to 10% for the second mode, whereas the TLM deviations range from 6.4% for the first mode to 13% fourth mode. Soriano et al. associate the FDTD deviations partially to inherent numerical errors of FDTD and the Fast Fourier Transform sensitivity, but primarily to the fact that their model does not include both day and nighttime ionospheric conditions.

The third group, in [Yang and Pasko 2005], also studies SRs using initially an azimuthally-symmetric 3-D FDTD model of the Earth-ionosphere cavity. Their model extends to an altitude of 100 km with a resolution of 1,000 x 1,000 x 2.5 km. They assume a PEC ground and test four different ionosphere conductivity profiles: (1) an ideal, free space cavity with a PEC ionosphere boundary; (2) a single-exponential profile with perturbation [Sentman 1983]; (3) a two-exponential profile using the same scale height for both sections [Sentman 1990, Greifinger and Greifinger 1978, Mushtak and Williams 2002]; and (4) a "knee" profile [e.g. Mushtak and Williams 2002]. Yang and Pasko excite their grid with a lightning current source and calculate the first five SR frequencies and associated Q factors from the radial *E*-field power spectrum at a

distance of 2 Mm. Fig. 6 (courtesy of [Yang and Pasko 2005]) shows the predicted shifts in the first Schumann resonance eigenfrequency (a) and Q-factor (b) as a function of the altitude (z_0) of the perturbation in the single-exponential ionosphere conductivity profile. Good agreement is obtained between the 3-D azimuthally symmetric FDTD model predictions described in [Yang and Pasko 2005] and the analytical (mode theory) results of [Sentman 1983]. In [Yang and Pasko 2005], the "knee" profile is shown to provide the most accurate results compared to the theoretical model of [Ishaq and Jones 1977]. If a three-scale model of the ionospheric conductivity were to be used in Yang and Pasko's FDTD model, it is expected that the FDTD-calculated results for SR frequencies and Q-factors would be even more accurate [Mushtak and Williams 2002].

Next, in [Yang and Pasko 2005], SRs for disturbed conditions associated with solar proton events and X-ray bursts are investigated. The solar proton event is modeled as azimuthally symmetric conductivity perturbations at an altitude of 40 km and centered at the North and South Poles; the X-ray burst is modeled as an azimuthally symmetric conductivity perturbation at an altitude of 70 km and centered only at the North Pole. A discussion follows comparing the FDTD-calculated results with previous reports in the literature [Sentman 1983, Schlegel and Fuellekrug 1999, Roldugin et al. 2001, Roldugin et al. 2003]. Overall, Yang and Pasko find that conductivity perturbations at high altitudes (>70 km) lead to an increase in the first SR frequency and conductivity perturbations at low altitudes (<70 km) lead to a decrease in the first SR frequency.

In [Navarro et al. 2008], the authors also conduct FDTD studies involving solar proton events and x-ray bursts using their previous azimuthally symmetric model of the Earth-ionosphere waveguide with a PEC ground. However, relative to their previous work of [Soriano

et al. 2005], they utilize an azimuthally-symmetric ionosphere derived from the International Reference Ionosphere (IRI) model, and they extend the model up to 180 km. Relative to [Yang and Pasko 2005], [Navarro et al. 2008] instead obtain the resonant "pure" (non-degenerate) SR and their frequencies for each study. This approach provides additional insight into the frequency shifts and distribution of the fields around the Earth for each SR under various ionospheric conditions during solar proton events and x-ray bursts. The pure SRs (excitation of which is impossible in the real world) is found by using the spatial distribution of the calculated mode, and repeating simulations until convergence is achieved.

Later, in [Yang and Pasko 2006] and [Yang and Pasko 2007], diurnal and seasonal variations of the power of the first Schumann resonance are investigated. For these studies, a fully 3-D FDTD model of the Earth-ionosphere waveguide (i.e. no longer azimuthally symmetric) is used having an ionospheric conductivity profile derived from the International Reference Ionosphere (IRI) [Bilitza 2001] above 60 km. Lightning sources are modeled as varying between the three major lightning storm regions of the world (The Maritime Continent, Africa, South America) depending on the time of day, and a receiver is located in the Negev Desert, Israel. The primary conclusion of [Yang and Pasko 2006] is that the recorded SR power and frequency variation changes with the local and universal time, as well as with the position of the receiver with respect to the lightning centers (since the height of the ionosphere changes with time of day, and each of the major lightning storm region activity varies with time of day). The overall behavior of their calculated FDTD results agrees well with the experimental data of [Price and Melnikov 2004].

In [Yang and Pasko 2007], the authors expand the work of [Yang and Pasko 2006] to account for El Nino and La Nina phenomena (the positions of the simulated major lightning

storm locations are shifted southward and northward, respectively). They clearly observe different power variation patterns in the electrical and magnetic components, and their results agree qualitatively with the experimental measurements of [Satori and Zieger 1999]. Additionally, they propose a method of detecting the spatial shifts in the thunderstorm regions using a combination of electric and magnetic components at a single recording station.

In [Yang et al. 2009], the work of [Yang and Pasko 2006] is taken a step further to inversely calculate the intensity of lightning in the Maritime Continent, Africa and South America regions using the genetic algorithm optimization method, an optimization and search technique based on the principles of genetics and natural selection [Haupt and Haupt 2004]. In [Yang and Pasko 2006], the lightning activity data are taken from previously published sources. But in [Yang et al. 2009], the lightning activity during different seasons are inversely calculated from experimental SR power measurements at SR field stations [e.g., Price and Melnikov 2004]. Optical Transient Detector (OTD) satellite measurements are utilized to evaluate the Yang et al. results.

Finally, in two additional publications, SRs on other planetary bodies are investigated, including Titan (Saturn's largest moon), Mars, and Venus [Yang et al. 2006], and again on Mars [Soriano et al. 2007]. Understanding SRs on planetary bodies such as Titan could help support the existence of electrical discharges and provide other useful information regarding its lower ionosphere [Yang et al. 2006]. These studies of other planetary bodies will not be described in detail in this Paper, but they are noted here as being very interesting and useful applications of the same techniques applied here to the Earth-ionosphere waveguide.

B. HYPOTHESIZED PRE-SEISMIC LITHOSPHERE SOURCES AND RADIATION

Anomalous EM wave phenomena occurring prior to major earthquakes have been of particular interest for many years (see for example [Park et al. 1993, Johnston 1997]). A number of physical mechanisms related to hypothetical earthquake precursors have been proposed to explain the origin of such observations, including electrokinetic effects, piezoelectric effects, magnetohydrodynamic effects, charge generation processes, etc. (see for example [Johnston 1997]). However, the existence and characteristics of any pre-seismic EM signatures remain unclear and very controversial.

Simpson and Taflove [2005a] use their global 3-D FDTD model described in [Simpson and Taflove 2004a] and Section II(C) to model one of the possible mechanisms, electrokinetic currents, at depths of 2.5 km and 17 km near the hypocenter of the California 1989 Loma Prieta earthquake. They compare the FDTD-calculated surface magnetic field to analytical results and measurements previously reported in the literature [Fenoglio et al. 1995, Mojaeva et al. 1997, Fraser-Smith et al. 1990]. Unlike previous analytical studies of this phenomena [Fenoglio et al. 1995, Mojaeva et al. 1997], the full Maxwell's equations FDTD model accommodates the complete physics introduced by impulsive EM wave propagation through the conductive Earth, as well as EM wave reverberation due to round-the-world propagation. As a result, Simpson and Taflove obtain a significantly different (more accurate) temporal response at the Earth's surface than that of [Fenoglio et al. 1995, Mojaeva et al. 1997].

Later, in [Simpson 2008], Simpson builds upon the initial investigation of anomalous pre-seismic EM signals in [Simpson and Taflove 2005a] by examining propagation from electric current sources buried at various depths and having different orientations in the Earth's crust. This study may actually be considered relevant to any currents occurring in the Earth's crust, independent of the mechanism involved in generating those currents.

Specifically, again employing the 3-D latitude-longitude FDTD model of the Earth-ionosphere cavity as described in [Simpson and Taflove 2004a], the impulse response, or space-time Green's function, of the global Earth-ionosphere system is calculated for four different cases of an electric current source occurring below the epicenter of the Loma Prieta earthquake at 121.88° W, 37.04° N: (1) horizontal current source at 5 km depth; (2) horizontal current source at 17 km depth; (3) vertical current source at 3 km depth; (4) vertical current source at 14 km depth. Results for the surface horizontal magnetic field at the epicenter of the Loma Prieta earthquake are obtained for each of these current sources separately.

By way of calculating the impulse response of the entire Earth-ionosphere cavity, the EM time-waveform at any location may be obtained for arbitrary currents via convolution. Hence, the FDTD calculations may be used to better predict the orientation, depth, and duration of currents in the Earth's lithosphere from any signatures that may be present in measurement data. However, note that the impulse responses of [Simpson 2008] are for electric currents at specific depths below the epicenter of the Loma Prieta earthquake. The calculated impulse response would not be valid for currents occurring at other depths or locations around the Earth (because the FDTD model includes the Earth's topography, electrical details of the continents and oceans, as well as both day- and night-time conditions of the ionosphere).

The results of [Simpson 2008] indicate that the choice of alignment and depth of the electric current within the Earth's crust yields significant differences for the calculated surface magnetic field time-waveforms. For example, the late-time response of the deeper, both vertical and horizontal sources are of higher magnitude than those of the shallower sources due to the longer diffusion time within the lossy crustal medium. Further, radiation from vertical sources nearer to the Earth's surface better couples into the transverse eletromagnetic (TEM) mode of the Earth-

ionosphere waveguide, which is capable of traveling completely around the Earth-ionosphere waveguide. Since the TEM mode travels around the Earth ~7 times each second with little attenuation, reverberations of the signal energy around the globe are more evident in magnetic-field recordings at the Earth's surface when the current source is at a shallower depth within the lithosphere.

More importantly, results of [Simpson 2008] indicate that, when assuming the Earth crustal conductivity values used in the FDTD model, EM fields recorded at the Earth's surface due to any hypothesized electric currents occurring in the Earth's crust at 5 km from the surface or deeper will only have significant spectra below ~1 Hz. This implies that any anomalous EM phenomena recorded in measurements around the world having spectra above ~1 Hz must be generated by other means, such as by ionospheric processes [Pulinets and Boyarchuk 2004] or by positive-charge carriers flowing in the Earth's crust that actually reach the Earth's surface as proposed in [Freund and Sornette 2007]. [Freund and Sornette 2007] proposes that a stressed rock volume can generate an outflow of defect electrons (known as positive holes or pholes for short). These pholes may possibly travel through adjacent unstressed rock, sand, and soil for up to km or tens of km towards the Earth surface. And once at the Earth's surface, these pholes may lead to a number of effects / phenomena, including infrared emissions and ionospheric perturbations.

Finally, the results of [Simpson 2008] indicate that it may be unlikely that the measured spectrum in [Fraser-Smith et al. 1990] prior to the Loma Prieta earthquake was caused by current sources within the lithosphere. The slope of the measured spectrum does not agree with the slopes of the calculated FDTD spectra for any of the orientations / depths of the lithosphere current sources considered. It is worth noting, however, that there are two factors [Simpson and

Taflove 2005a] that may be affecting the comparison of the FDTD-calculated spectrum with the measured Fraser-Smith data: (1) the assumed lithosphere conductivity values in the FDTD grid; and (2) a measurement artifact reported in [Fraser-Smith et al. 1990] wherein instrumentation saturation likely occurred at the lowest observed frequencies. In the first case, an excessive lithospheric conductivity would cause the FDTD-calculated spectra at higher frequencies to be unduly attenuated, thereby bending the calculated curves downward below the Fraser-Smith et al. data. In the second case, the Fraser-Smith et al. data point at lower frequencies would have too small a value relative to the actual values, thereby unduly flattening their measured spectra. As a result, since there are numerous examples of measured data having anomalous electromagnetic signals prior to and during earthquakes well above 1 Hz, other mechanisms aside from current sources in the lithosphere should be considered and studied in detail.

C. DETECTION OF DEEP UNDERGROUND RESOURCE FORMATIONS

Deep EM sounding of the Earth using controlled sources has been employed for decades as a means to determine the electrical properties of the Earth's lithosphere. Previously, controlled sources such as power lines, electrified railroads, and pulsed magnetohydrodynamic generators have been employed for such probing [Velikhov et al. 1998, Bashkuev 2001]. However, the data obtained from these methods exhibit an unsatisfactory, wide variance [Velikhov et al. 1998].

Since the early 1990's a promising new system for global remote sensing at frequencies below 300 Hz has been under investigation [Velikhov et al. 1998, Bashkuev 2001]. The advantages of using frequencies in this range for this application are: (1) a sufficiently large skin depth for deep probing (100 m and more in ocean and 10 km and more in crystalline shields); (2) low propagation attenuation, which could provide global remote sensing of the Earth with a

single source; (3) good stability compared to higher frequency methods that are more influenced by ionospheric disturbances [Velikhov et al. 1998].

The sounding methodology described in [Velikhov et al. 1998, Bashkuev 2001], however, involves EM field impedance measurements to determine the resistivity of the underlying rock. This requires measurement of both the tangential electric and the tangential magnetic fields near the Earth's surface. In [Simpson et al. 2006, Simpson and Taflove 2005b], a novel subsurface radar working at frequencies below 76 Hz is proposed that does not involve impedance measurements. This radar is designed to sense the presence of major oil deposits by recording instead only the radial magnetic field above the Earth's surface. To illustrate the new global detection technology, the FDTD grid simulates a quasi-sinusoidal pulse radiated outward from the former U.S. Navy Wisconsin Transmitting Facility (WTF). Signal acquisition and processing is facilitated by the well-characterized nature of the source and the proposed use of aerial surveys employing SQUID magnetometers [Lee et al. 2002].

As an example, Simpson and Taflove report numerical simulations of radar returns from a hypothetical Alaskan oilfield excited by a pulsed 20-Hz quasi-sinusoidal signal emitted from the WTF. Using their 3-D geodesic and latitude-longitude whole-Earth FDTD propagation models described in Section II(C) [Simpson et al. 2006, Simpson and Taflove 2005b], they show that detection of the radial (vertical) component of the scattered magnetic field exhibits an unexpected and very high degree of sensitivity to the presence of deeply buried conductivity anomalies of the lithosphere, much more so than the tangential magnetic field. They propose exploiting this phenomenon to establish a means to rapidly and inexpensively conduct aerial surveys of thousands of square km for significant oilfields.

UU IR Author Manuscript

D. REMOTE SENSING OF LOCALIZED IONOSPHERIC ANOMALIES

Despite substantial ground and satellite-based technology for studying the upper ionosphere, extracting the electron densities versus height in the D-region (< 95 km) is still a difficult problem, particularly at night [Cummer et al. 1998]. For example, measurement techniques have included in-situ probing by rockets [Sechrist 1974] and remote sensing of radiated spectra generated by random, naturally occurring sources, such as lightning [Cummer 1998]. However, these methods may not provide a practical means of continuously monitoring the lower ionosphere, and may be difficult or impossible to implement in many regions of the world. As a result, alternative techniques are needed in order to measure and analyze anomalous behavior of the D-region due to geophysical, solar, or other phenomena.

In [Simpson and Taflove 2006], a novel radar working at 76 Hz is proposed for locating and characterizing localized ionospheric anomalies within ~100 km of the Earth's surface. Their system assumes operation of the WTF as a distant, well-characterized, pulsed sinusoidal source, and passive detection of the resulting vertical electric field time-waveform at the Earth's surface in the vicinity of the ionospheric anomaly. Employing a man-made source such as the WTF could allow, in principle, a continuous and systematic monitoring scheme that avoids variabilities arising from naturally occurring sources such as lightning which have random properties.

To illustrate the operation of their proposed system, [Simpson and Taflove 2006] provides three calculations of vertical electric field signals at the Earth's surface in Los Angeles below bowl-shaped ionospheric conductivity depressions using their 3-D geodesic-grid whole-Earth FDTD wave propagation model described in [Simpson et al. 2006] and Section II(C). The depressions are assumed to have a depth of 20 km and a radius of either 100 km, 200 km, or 380

km. Remote excitation is provided by a 76-Hz sinusoidal pulse radiated essentially isotropically from the WTF. The FDTD-calculated results show that a simple measurement of the vertical electric field signal below a localized ionospheric depression can provide its location, size, shape, and depth. The radar proposed in [Simpson and Taflove 2006] could therefore provide useful information regarding localized ionospheric depressions hypothesized to occur as earthquake precursors [Simpson 2007, Pulinets and Boyarchuk 2004], as well as other local ionospheric conditions relating to geophysical processes.

III. FUTURE POSSIBILITIES FOR THE 3-D GLOBAL FDTD MODELS

This Section provides some example areas that may benefit from ongoing and future research involving 3-D global FDTD models. Advancements and applications that may come about as computing technologies continue to improve in the coming years and decades are provided.

A. GYROTROPIC IONSOPHERIC PLASMA

The ionosphere is known to be highly anisotropic due to the influence of the geomagnetic field upon the ionosphere's electron and ion constituents [Hu and Cummer 2006]. An isotropic ionosphere having an exponential conductivity profile as used in many of the FDTD models described in previous sections of this Paper appears to be adequate in calculating the average propagation of EM waves at frequencies less than ~1 kHz over thousands of km [Simpson and Taflove 2007]. However, its inability to incorporate such effects as Faraday rotation limits its accuracy in calculating details of higher-frequency EM energy as radiated by lightning and sprites within a range of 1000 km of the atmospheric excitation, or in modeling ionospheric processes above ~100 km.

UU IR Author Manuscript

One area of ongoing work is to advance the 3-D FDTD global grids described in [Simpson and Taflove 2004a, Simpson et al. 2006] and Section II(C) to model frequency-dispersive, anisotropic magnetized ionosphere plasma [Yu and Simpson, submitted]. These new models will include global geomagnetic data, and will yield region-specific ionospheric propagation results around the globe (i.e. polar regions vs. equatorial regions and variations with time of day, in addition to the variation in propagation already introduced by the Earth's topography / bathymetry).

The first step in generating the global Earth-plasma ionosphere models is to extend the models well beyond their previous upper boundary limit of 100 km in altitude. The lower grid boundary of 100 km below sea level will be maintained so that EM interaction studies closer to DC may still be conducted. (At sufficiently low frequencies, the EM energy can penetrate much of the Earth's conductive lithosphere and upon reflection from any discontinuities, reflect and reenter the Earth's atmosphere. But even at a frequency of 0.01 Hz, the skin depth of a lithosphere volume having an average conductivity of 0.02 S/m is on the order of 60 km, so that the 100-km-thick modeled lithosphere sufficiently attenuates the 0.01 Hz EM wave.) The resulting FDTD software will thus be very broadband.

Next, input data for the ionosphere will be required. First, the freely available International Reference Ionosphere (IRI) [Online: http://modelweb.gsfc.nasa.gov/ionos/iri.html] will be used to obtain the density profiles of electrons and ions in relation to altitude, position on the Earth, as well as date and time of day. Second, the collision frequencies at varying altitudes will be calculated using [Cummer 1997, Hu and Cummer 2006] and references therein. Third, the Earth's magnetic field data will be obtained from the International Geomagnetic Reference

Field (IGRF) offered freely through the Internet by the National Geophysical Data Center (NGDC) [Online: http://www.ngdc.noaa.gov/seg/geomag/models.shtml].

The final step in generating the global Earth-plasma ionosphere models is to incorporate a gyrotropic plasma algorithm into the ionosphere section of the FDTD grid. For this step, the 2-D cylindrical-coordinate FDTD plasma algorithm of [Hu and Cummer 2006] has been chosen because other FDTD plasma models have been found to introduce a late-time instability into the code, require a time step several orders of magnitude smaller than that necessitated by the Courant limit of the grid for numerical stability, or require a significant amount of additional storage and time for processing [Yu and Simpson, submitted]. Further, Hu and Cummer have attained good agreement at both high altitudes and over long distances between experiments / mode theory and their 2-D model results. However, unlike for their 2-D model, a 3-D model provides additional capabilities, such as the modeling of Faraday rotation effects and the inclusion of fully 3-D spatial variations in the magnetization and characteristics of the cold plasma.

Working towards fully 3-D global FDTD plasma-ionosphere models, an initial 3-D Cartesian-coordinate magnetized cold plasma model has been generated and submitted for publication [Yu and Simpson, submitted]. This model is validated by testing the Faraday rotation and other propagation characteristics of a linearly-polarized plane (along the x-axis) wave propagating in the z-direction. The Faraday rotation effect is demonstrated in Fig. 7, which shows tracings of the total electric field vectors at different recording points along the direction of propagation for an applied magnetic field of 1.7T. These tracings show the rotation of the linearly polarized wave, and they are obtained by plotting the recorded E_x and E_y values over one cycle using the electric field magnitudes as the x-y coordinates. The wave rotates at a constant

rotation angle per unit distance that agrees very well with plasma theory [Chen 1984].

In ongoing and future work, the Cartesian-coordinate magnetized plasma model will be adapted to the 3-D global latitude-longitude and geodesic FDTD models of [Simpson and Taflove 2004a, Simpson et al. 2006] and Section II(C). For the latitude-longitude grid, the adaptation of the 3-D Cartesian-coordinate plasma model will involve a non-trivial re-derivation of the plasma updating coefficients mapped into the regular trapezoidal and triangular cells of the FDTD grid, as well as the eccentric West-East merged cells in the polar regions as required for numerical efficiency. For the geodesic grid, the adaptation will require a complete re-derivation of the plasma updating coefficients for the hexagonal / pentagonal cells. However, realization of these final combined EM wave / ionospheric physics models would represent a fundamental advancement in geophysics, and they could subsequently be used in a wide variety of research areas. Two such areas are discussed in the following sub-sections.

B. LIGHTNING SOURCES AND RADIATION

The 2-D studies described in Section II(B) involving propagation from lightning and FDTD modeling of trimpis (whistlers, sprites, elves) is an area of research that could immediately benefit from the work described in Section III(A). First, the previous 2-D lightning work could be expanded to fully 3-D FDTD models of the Earth-ionosphere waveguide that incorporate the Earth's magnetic field and ionospheric plasma. Then, these 3-D models could be expanded to a global scale, so that a multitude of broadband lightning sources, radiation, and localized / global propagation studies could be studied around the world simultaneously. These models would require memory-intense, high-resolution grids, but they would be able to account for both large- and small-scale ionospheric disturbances, topographical variations, ocean-continent propagation

effects, and ionospheric variations and variations in lightning phenomena between the polar and equatorial regions, to name a few. Furthermore, as the FDTD models are extended to higher altitudes relative to the highest modeling altitude provided by previous FDTD simulations, additional lightning strikes occurring at higher altitudes may also be included.

C. SPACE WEATHER EFFECTS

The incorporation of the geomagnetic field and ionospheric plasma physics into global 3-D FDTD models, as well as advancing these models to higher resolutions and higher altitudes, could also significantly help advance the understanding of space weather affects on the Earth and ionosphere. One example within this topic that will be discussed here is in the area of coronal mass ejections (CMEs).

The historical record indicates that extraordinarily intense CMEs are possible. The largest documented CME occurred in 1859 [Shea et al. 2006]. This CME caused telegraph operators communicating over 100-km-long wire lines to experience electric shocks, some nearly fatal [Odenwald 2002]. Further, business transactions requiring telegraphic exchanges were completely shut down in the world's major capitals [Odenwald 2002].

It is clear that the occurrence of an 1859-magnitude CME could disrupt today's human society to a much greater degree than in 1859 due to the proliferation of vital but vulnerable electrotechnologies. Interruptions to radio communications, satellite operations, home and industrial computer electronics, and power grids are just a few examples [Odenwald and Green 2008].

The effects of CMEs on power grids can be extreme. [Kappenman et al. 1997] warns, "the sprawling North American power grid resembles a large antenna, attracting electrical currents

induced by giant solar storms. Severe space weather occurring during solar cycles has the potential to cause a large-scale blackout in North America." To exacerbate this issue, for many years following a relatively quiet 30-year period, electrical power distribution transformers were designed to be less tolerant to space weather events [Kappenman et al. 1997]. Further, current protective technologies cost in the billions of dollars, which discourages power companies from taking effective preventative measures [Kappenman et al. 1997]. As a result, a March 1989 CME caused the HydroQuebec power grid to fail for about nine hours, resulting in disruptions to hospital and emergency operations, as well as transportation, public security, and production [Kappenman et al. 1997]. Thus, even "based on the sole impact of the smaller but famous March 1989 storm on the North American power transmission system (e.g., [Czech et al. 1989], [Bolduc 2002]), it is safe to say that geomagnetically induced currents (GICs) [are] one of the most important space weather hazards" [Pulkkinen et al. 2007]. And, a "need for science-based mitigation capabilities is real" [Pulkkinen et al. 2007].

FDTD modeling could be utilized to enhance on a global scale the understanding of broadband electrodynamics associated with historically intense CMEs. Such modeling would be an advance relative to essentially all relevant published analytical and computational models. FDTD models can simultaneously (1) accommodate EM wave propagation dynamics within the global Earth-ionosphere cavity (i.e. solve the complete set of Maxwell's equations); (2) examine EM phenomena throughout a wide range of frequencies simultaneously; (3) account for effects introduced by the Earth's topography / bathymetry (such as the build-up of GICs at the interfaces of low-conductivity continental masses and high-conductivity ocean basins [Olsen and Kuvshinov 2004], which is thought to affect regions on the order of tens to a few hundred km [Pirjola 2000], but is an issue not yet fully understood, and "requires additional modeling studies

for more quantitative conclusions" [Pirjola 2000]); (4) account for effects introduced by the 3-D variability of the lithosphere composition data (such as regions of highly resistive igneous rock where power systems are the most vulnerable [Kappenman et al. 1997]); (5) account for effects introduced by both day- and nighttime ionospheric conditions and transitions (such as variations in the electron and ion content and the downward or upward radial flow of field-aligned currents with regards to position around the Poles [Bothmer and Daglis 2007]); and (6) account for effects introduced by the global geomagnetic data (which will contribute to differing EM effects in the polar regions versus the equatorial regions).

No analytical or computational techniques published to date are capable of accommodating all of the above six capabilities permitted by the FDTD modeling. For example, [Shao et al. 2002] employs a magnetohydrodynamic (MHD) ionosphere model and the Biot-Savart Law (magnetostatic approximation) to project magnetic fields onto the Earth's surface, and [Pulkkinen et al. 2007] employs an MHD model along with complex-image theory to calculate the magnetic fields at the Earth's surface. Neither of these methods solves the full / complete Maxwell's equations nor provides capabilities (2) – (4) from the above list. Another example, [Shepard and Shubitidze 2003], makes use of the method of auxiliary sources (MAS), which does permit some 2-D or 3-D geometrical inhomogeneities, but is limited by the size of the resulting matrix equations and also does not solve the complete Maxwell's equations (neglects displacement currents). Thus, FDTD modeling would yield a much more rigorous and realistic analyses of the dynamics involved in the interaction of a CME with the Earth-ionosphere environment.

In particular, global FDTD models may be employed to calculate induced electric and magnetic fields in the ionosphere and at the Earth's surface due to ionospheric currents induced

by the CME. Output data would include finely detailed region-specific predictions of the behavior of ground-level magnetic fields and potential rises, especially in areas of highly resistive lithosphere rock and along continent-ocean boundaries. These data may provide engineers improved information to help them assess potential hazards and devise less expensive counter technologies / improved contingency plans for the most vulnerable sections and components of power grids under a wide variety of ionospheric conditions.

In the Aug. 2008 issue of Scientific American [Odenwald and Green 2008] is writen, "… scientists have a long way to go to understand the physics of solar storms and to forecast their effects. If we really want to safeguard our technological infrastructure, we will have to redouble our investment in forecasting, modeling, and basic research to batten down for the next solar tempest." Global FDTD modeling is one step that may help both in gaining a better physical understanding and in helping protect the world's technological infrastructure.

D. MULTI-PHYSICS SOFTWARE SUITE

Future work could also include self consistently linking global FDTD simulators to sophisticated ionosphere models, such as the U.S. Naval Research Lab's SAMI3 [Online: http://www.nrl.navy.mil/content.php?P=04REVIEW105]. This would yield multiphysics software suites encompassing many fields of research. For example, in addition to solving the full Maxwell's equations using FDTD, the addition of SAMI3 would model the plasma and chemical evolution of seven ion species between altitudes of 85 km to 20,000 km [Online: http://www.ngdc.noaa.gov/seg/geomag/models.shtml]. Furthermore, SAMI3 has already been coupled with a variety of numerical simulators, such as the solar-wind-magnetosphere Lyon-Fedder-Mobarry (LFM) model of the solar wind/magnetosphere system [Chen et al. 2008], and

the Rice Convection Model (RCM) of the inner magnetosphere that includes coupling to the ionosphere [Huba 2007]. As a result, a future FDTD-SAMI3-LFM-RCM multiphysics software suite could provide a wide variety of possibilities for realistic modeling of space weather effects and Earth-ionosphere-magnetopshere dynamics.

IV. CONCLUSION

This Paper has provided a historical overview of the emergence of fully 3-D global FDTD models of the Earth-ionosphere system. These FDTD models have begun to take advantage of the availability of large-scale computational resources to investigate much more complex EM wave interactions within the lithosphere, oceans, and ionosphere than was possible using previous analytical models. Descriptions of previous and current applications of these FDTD models, including lightning sources and radiation, Schumann resonances, hypothesized pre-seismic lithosphere sources and radiation, detection of deep underground resource formations, and remote sensing of localized ionospheric anomalies have been provided. And finally, possibilities for ongoing and future work in this area are discussed, such as in modeling the gyrotropic plasma ionosphere on a global scale, modeling lightning sources and radiation, investigating space weather effects, and linking FDTD models with other types of models to generate multi-physics software suites. Indeed, FDTD modeling of the Earth and its ionosphere is expected to expand in the coming years and decades as computing infrastructures continue to improve.

REFERENCES:

UU IR Author Manuscript

Ando Y, Hayakawa M, Shvets A V, Nickolaenko A P (2005) Finite difference analyses of Schumann resonance and reconstruction of lightning distribution. Radio Sci. 40(2), doi: 10.1029/2004RS003153.

Bannister P (1984) ELF propagation update. IEEE Journal of Oceanic Eng. 0E-9(3):179 - 188.

Bannister P (1985) The determination of representative ionospheric conductivity parameters for ELF propagation in the Earth-ionosphere waveguide. Radio Sci. 20 (4):977 - 984.

Bashkuev Y B, Khaptanov V B (2001) Deep radio impedance sounding of the crust using the electromagnetic field of a VLF radio installation. Izvestiya – Phys. of the Solid Earth 37(2):157-165.

Berenger J P (1994a) Finite-difference computation of VLF-FL propagation in the Earth-ionosphere waveguide. EUROEM Symposium, Bordeaux, France.

Berenger J P (1994b) A perfectly matched layer for the absorption of electromagnetic waves. J. Computational Physics 114:185-200.

Berenger J P (2002a) Reduction of the angular dispersion of the FDTD method in the Earth-ionosphere waveguide. Journal Electromagnetic Waves and Applications 17(8):1225-1235.

Berenger J P (2002b) FDTD computation of VLF-LF propagation in the Earth-ionosphere waveguide. Annals of Telecommunications 57(11-12):1059-1090.

Berenger J P (2004) On the reflection from Cummer's nearly perfectly matched layer. IEEE Microwave Wireless Lett. 14(7):334-336.

Berenger J P (2005) Long-range propagation of lightning pulses using the FDTD method. IEEE Transactions on Electromagnetic Compatibility 47(4):1008 – 1012.

Bilitza D (2001) IRI 2000. Radio Science 36(2):261-276.

Bothmer V, Daglis I A (2007) Space Weather: Physics and Effects, Springer: New York, NY.

Bruce C E R, Golde R H (1941) The lightning discharge. J. Inst. Electr. Eng. 88:487-505.

Chen F F (1984) Introduction to Plasma Physics and Controlled Fusion, 2nd ed., New York Plenum Press.

Chen J, Huba J D, Slinker S (2008) An accurate real-time method of predicting storm-time global ionospheric dynamics using 1 AU solar-wind data. Fifth Symposium on Space Weather, American Meteorological Society.

Cooray V (1992) Horizontal fields generated by return strokes. Radio Sci. 27:529-537.

Cummer S A (1997) Lightning and ionospheric remote sensing using VLF/ELF radio atmospherics. Ph.D. Thesis, Stanford University.

Cummer S A (2000) Modeling electromagnetic propagation in the Earth-ionosphere waveguide. IEEE Trans. Antennas Propagation 48(9):1420.

Cummer S A (2003) A simple, nearly perfectly matched layer for general electromagnetic media. IEEE Microwave and Wireless Lett. 13:128-130.

Cummer S A, Inan U S, Bell T F (1998) Ionospheric D region remote sensing using VLF radio atmospherics. Radio Sci. 33:1781-1792.

Fenoglio M A, Johnston M J S, Byerlee J D (1995) Magnetic and electric fields associated with changes in high pore pressure in fault zones: application to the Loma Prieta ULF emissions. J. Geophs. Res. 100:12951-12958.

Fraser-Smith A C, Bernardi A, McGill P R, Ladd M E, Helliwell R A, Villard O G Jr. (1990) Low-frequency magnetic field measurements near the epicenter of the Ms 7.1 Loma Prieta earthquake. Geophys. Res. Lett.17:1465-1468.

Freund F, Sornette D (2007) Electro-magnetic earthquake bursts and critical rupture of peroxy bond networks in rocks. Tectonophysics 431:33-47.

Greifinger C, Greifinger P (1978) Approximate method for determining ELF eigenvalues in the Earth-ionosphere cavity. Radio Sci. 13:831.

Haupt R L, Haupt S E (2004) Practical Genetic Algorithms. John Wiley. Hoboken, NJ.

Hayakawa M, Otsuyama T (2002) FDTD analysis of ELF wave propagation in inhomogeneous subionospheric waveguide models. ACES Journal 17(3):239-244.

Hermance J (1995) Electrical conductivity of the crust and mantle. Global Earth Physics: A Handbook of Physical Constants, AGU.

Holland R (1983) THREDS: A finite-difference time-domain EMP code in 3-D spherical coordinates. IEEE Trans. Nucl. Sci., vol. NS-30(6):4592-4595.

Hu W, Cummer S A (2006) An FDTD model for low and high altitude lightning-generated EM fields. IEEE Trans. Antennas Propag. 54(5):1513-1522.

Hu W, Cummer S A, Lyons W A (2007) Testing sprite initiation theory using lightning measurements and modeled electromagnetic fields. Journal of Geophysical Research. 112:D13115, doi:10.1029/2006JD007939.

Huba J D (2007) Ionospheric modeling: coupling to the inner and outer magnetosphere. American Geophysical Union Joint Assembly, Acapulco, Mexico.

Ishaq M, Jones D L (1977) Method of obtaining radiowave propagation parameters for the Earth-ionosphere duct at ELF. Electron. Lett. 13:254.

Johnston M J S (1997) Review of electric and magnetic fields accompanying seismic and volcanic activity. Surv. Geophys., 18:441-475.

Kappenman J G, Zanetti L J, Radasky W A (1997) Geomagnetic storms can threaten electric power grid. Earth in Space 9(7):9-11.

Kellali S, Jecko B, and Reineix A (1993) Implementation of a surface impedance formalism at oblique in FDTD method. IEEE Trans. Electromagn. Compat. 35:347-356.

Kuo C-L, Chen A B, Lee Y L, et al. (2007) Modeling elves observed by FORMOSAT-2 satellite. Journal of Geophysical Research, 112:A11312, doi:10.1029/2007JA0124007.

Lee J B, Dart D L, Turner R J, et al. (2002) Airborne TEM surveying with a SQUID magnetometer sensor. Geophysics 67(2):468-477.

Majaeva O, Fujinawa Y, Zhitomirsky M E (1997) Modeling of non-stationary electrokinetic effect in a conductive crust," J. Geomag. Geoelectr. 49:1317-1326.

Maloney J G, Smith G S (1992) The use of surface impedance concepts in the finite-difference time-domain method. IEEE Trans. Antennas Propag. 40:38-48.

Morente J, Molina-Cuberos J, Porti J, Besser B, Salinas A, Schwingenschuch K, Litchengger H (2003) A numerical simulation of Earth's electromagnetic cavity with the transmission line matrix method: Schumann resonances. J. Geophys. Res. 108(A5).

Mushtak V C, Williams E (2002) ELF propagation parameters for uniform models of the Earth-ionosphere waveguide. J. Atmos. Sol. Terr. Phys. 64(18):1989-2001.

Navarro E A, Soriano A, Morente J A, Porti J A (2008) Numerical analysis of ionosphere disturbances and Schumann mode splitting in the Earth-ionosphere cavity. Journal of Geophysical Research 113:A09301, doi:10.1029/2008JA013143.

Nickolaenko A P, Hayakawa M (1998) Natural electromagnetic pulses in the ELF range. Geophys. Res. Lett. 25(16): 3101-3106.

Nickolaenko A P, Hayakawa M (2002) Resonances in the Earth-Ionosphere Cavity, Kluwer Academic Publishers, Dordrecht.

Nickolaenko A P, Hayakawa M, Kudintseva I G, Myand S V, Rabinowicz L M (1999) ELF sub-ionospheric pulse in time domain. Geophys. Res. Lett. 26:999-1002.

Odenwald S (2002) The 23rd Cycle: Learning to Live with a Stormy Star, Columbia University Press.

Odenwald S F, Green J L (2008) Bracing for a solar superstorm. Scientific American 299(2):80-87.

Olsen N, Kuvshinov A (2004) Modeling the ocean effect of geomagnetic storms. Earth Planets Space 56:525-530.

Otsuyama T, Hayakawa M (2002) FDTD simulation and experimental result on VLF scattering by ionospheric perturbations in Earth-ionosphere waveguide. T. IEE. Japan 122-A(1):59 – 63.

Otsuyama T, Hayakawa M (2004) FDTD Analysis of ELF wave propagation for realistic subionospheric waveguide models. IEEJ Trans. FM 124(12):1203-1209.

Pappert R A, Ferguson F A (1986) VLF/LF mode conversion model calculations for air to air transmissions in the Earth-ionosphere waveguide. Radio Science 21(4):551.

Park S K, Johnston M J S, Madden Th R, Morgan F D, Morrison H F (1993) Electromagnetic precursors to earthquakes in the ULF band: a review of observations and mechanisms. Rev. Geophys. 31:117-132.

Pechony O, Price C (2004) Schumann resonance parameters calculated with a partially uniform knee model on Earth, Venus, Mars, and Titan. Radio Sci. 39(5).

Pirjola R (2000) Geomagnetically induced currents during magnetic storms. IEEE Transactions on Plasma Science 28(6):1867 – 1873.

Poussard A M, Corcuff Y (2000) Numerical simulation of LEP Trimpis observed at Poitiers France, on signals from VLF transmitters. Journal of Atmospheric and Solar-Terrestrial Physics 62: 207-224.

Price, Melnikov (2004) Diurnal, seasonal, and inter-annual variations of the Schumann resonance parameters. Journal Atmospheric Solar-Terrestrial Physics 66(13- 14):1179-1185.

Pulinets S, Boyarchuk K (2004) Ionospheric Precursors of Earthquakes, Berlin, Germany: Springer.

Pulkkinen A, Hesse M, Kuznetsova M, Rastätter L (2007) First principles modeling of geomagnetically induced electromagnetic fields and currents from upstream solar wind to the surface of the Earth. Annales Geophysicae 25(4):881-893.

Randall D A, Ringler T D, Heikes R P (2002) Climate modeling with spherical geodesic grids. Computing in Science and Engineering 4(5):32 – 41.

Roldugin V C, Maltsev Y P, Petrova G A, Vasiljev A N (2001) Decrease of the first Schumann resonance frequency during solar proton events. J. Geophys. Res. 106: 18,555.

Roldugin V C, Maltsev Y P, Vasiljev A N, Schokotov A Y, Belyajev G G (2004) Schumann resonance frequency incrase during solar X-ray bursts. J. Geophys. Res. 109(A01216) doi:10.1029/2003JA010019.

Roldugin V C, Maltsev Y P, Vasiljev A N, Shvets A V, Nikolaenko A P (2003) Changes of Schumann resonance parameters during the solar proton event of 14 July 2000. J. Geophys. Res. 108(A3):1103, doi:10.1029/2002JA009495.

Rubinstein M (1996) An approximate formula for the calculation of the horizontal electric field from lightning at close, intermediate, and long range. IEEE Trans. Electromagn. Compat. 38:531-535.

Sarto M S (2001) Innovative absorbing-boundary conditions for the efficient FDTD analysis of lightning-interaction problems. IEEE Trans. Electromagnetic Compatibility 43(3):368.

Satori G, Zieger B (1999) El Nino related meridional oscillation of global lightning activity. Geophys. Res. Lett. 26:1365.

Schlegel K, Fuellekrug M (1999) Schumann resonance parameter changes during high-energy particle precipitation. J. Geophys. Res.104(A5):10111-10118.

Schlegel K, Fuellekrug M (1999) Schumann resonance parameter changes during high-energy particle precipitation. J. Geophys. Res. 104:10-11.

Schumann W O (1952) On the radiation free self-oscillations of a conducting sphere, which is surrounded by an air layer and an ionospheric shell [in German]. Zeitschrift fuer Naturforschung 7a:149-154.

Sechrist C F Jr (1974) Comparisons of techniques for measurement of D-region electron densities. Radio Science 9:137.

Sentman D D (1983) Schumann resonance effects of electrical conductivity perturbations in an exponential atmospheric/iononspheric profile. J. Atmos. Terr. Phys. 45(1):55-65.

Sentman D D (1990) Approximate Schumann resonance parameters for two-scale height ionosphere. J. Atmospheric Terrestrial Phys. 52(1):35-46.

Sentman D D (1995) Schumann resonances, In Handbook of Atmospheric Electrodynamics, Ed. H. Volland 1:267-310, CRC Press.

Sevgi L, Akleman F, Felsen L B (2002) Groundwave propagation modeling: Problem-matched analytical formulations and direct numerical techniques. IEEE Antennas and Propagation Magazine 44(1):55 – 75.

Shao X, Guzdar P N, Milikh G M, et al. (2002) Comparing ground magnetic field perturbations from global MHD simulations with magnetometer data for the 10 January 1997 magnetic storm event. Journal of Geophysical Research-Space Physics, 107(A8):1177, doi:10.1029/2000JZ000445.

Shea M A, Smart D F, McCracken K G, et al. (2006) Solar proton events for 450 years: The Carrington event in perspective. Advances in Space Research 38(2):232-238.

Shepard S G, Shubitidze F (2003) Method of auxiliary sources for calculating the magnetic and electric fields induced in a layered Earth. Journal of Atmospheric and Solar-Terrestrial Physics 65:1151-1160.

Simpson J J (2008) Global FDTD Maxwell's equations modeling of electromagnetic propagation from currents in the lithosphere. IEEE Transactions on Antennas and Propagation 56(1):199-203.

Simpson J J, Heikes R P, Taflove A (2006) FDTD modeling of a novel ELF radar for major oil deposits using a three-dimensional geodesic grid of the Earth-ionosphere waveguide. IEEE Trans. Antennas Propag., 54(6):1734-1741.

Simpson J J, Taflove A (2002) Two-dimensional FDTD model of antipodal ELF propagation and Schumann resonance of the Earth. IEEE Antennas and Wireless Propagation Letters 1: 53-56.

Simpson J J, Taflove A (2004a) Three-dimensional FDTD modeling of impulsive ELF propagation about the Earth-sphere. IEEE Trans. Antennas and Propagation 52:443–451.

Simpson J J, Taflove A (2004b) Efficient modeling of impulsive ELF antipodal propagation about the Earth sphere using an optimized two-dimensional geodesic FDTD grid. IEEE Antennas and Wireless Propagation Letters 3(11):215-218.

Simpson J J, Taflove A (2005a) Entire-Earth FDTD Modeling of Electrokinetic Effects Prior to the Loma Prieta Earthquake. Geophysical Research Lett., 32:L09302, doi:10.1029/2005GL022601.

Simpson J J, Taflove A (2005b) A novel ELF radar for major oil deposits. IEEE Geoscience and Remote Sensing Letters 3(1):36-39.

Simpson J J, Taflove A (2006) ELF radar system proposed for localized D-region ionospheric anomalies. IEEE Geoscience and Remote Sensing Letters 3(4): 400-403.

Simpson J J, Taflove A (2007) A review of progress in FDTD Maxwell's equations modeling of impulsive sub-ionospheric propagation below 300 kHz. IEEE Transactions on Antennas and Propagation in the Special Issue on Electromagnetic Wave Propagation in Complex Environments: A Tribute to Leopold Benno Felsen 55(6):1582-1590.

Soriano A, Navarro E A, Morente J A, Porti J A (2007) A numerical study of the Schumann resonances in Mars with the FDTD method. Journal of Geophysical Research 112:A06311, doi:10.1029/2007JA012281.

Soriano A, Navarro E A, Paul D L, Porti J A, Morente J A, Craddock I J (2005) Finite-difference time domain simulation of the Earth-ionosphere resonant cavity: Schumann resonances. IEEE Trans. Antennas and Propagation 53(4):1535-1541.

Strangeways H J (1996) Lightning, Trimpis, and Sprites. Review Radio Science, 1993-1996, ed. R. Ross Stone, Oxford Univ. Press.

Taflove A (1980) Application of the finite-difference time-domain method to sinusoidal steady state electromagnetic penetration problems. IEEE Trans. Electromagnetic Compatibility 22:191-202.

Taflove A, Hagness S C (2005) Computational Electrodynamics: The Finite-Difference Time- Domain Method, 3rd. ed. Artech House MA.

Taflove A, Simpson J J (2005) Introduction to Maxwell's equations and the Yee algorithm. In Taflove A, Hagness S C (ed) Computational Electrodynamics: The Finite-Difference Time-Domain Method, 3rd edn, Artech House, MA.

Thevenot M, Berenger J P, Monediere Th, Jecko F (1999) A FDTD scheme for the computation of VLF-LF Propagation in the Anisotropic Earth-ionosphere Waveguide. Annals of Telecommunications 54(5-6):297-310.

Velikhov E P, Zhamaletdinov A A, Shevtsov A N, et al. (1998) Deep electromagnetic studies with the use of powerful ELF radio installations. Isvestiya, Physics of the Solid Earth 34(8):615-632.

Wait J R (1965) Earth-ionosphere cavity resonances and the propagation of ELF radio waves. Radio Science 69D:1057.

Williams E R (1992) The Schumann Resonance – a global tropical thermometer. Science 256:1184.

Williams E R (2005) Lightning and climate: A Review. Atmospheric Research 76(1-4):272-287.

Yang C, Zhou B (2004) Calculation methods of electromagnetic fields very close to lightning," IEEE Transactions on Electromagnetic Compatibility 46(1):133-141.

Yang H, Pasko V P (2005) Three-dimensional finite difference time domain modeling of the Earth-ionosphere cavity resonances. Geophys. Res. Lett. 32:L03114, doi:10.1029/2004GL021343.

Yang H, Pasko V P (2006) Three-dimensional finite difference time domain modeling of the diurnal and seasonal variations in Schumann resonance parameters. Radio Science 41:RS2S14, doi:10.1029/2005RS003402.

Yang H, Pasko V P (2007) Power variations of Schumann resonances related to El Nino and La Nina phenomena. Geophysical Research Letters 34:L11102, doi:10.1029/2007GL030092.

Yang H, Pasko V P, Satori G (2009) Seasonal variations of global lightning activity extracted from Schumann resonances using a genetic algorithm method. Journal of Geophysical Research. 114(E01103), doi:10.1029/2008JD009961.

Yang H, Pasko V P, Yair Y (2006) Three-dimensional finite difference time domain modeling of the Schumann resonance parameters on Titan, Venus, and Mars. Radio Science 1(2):RS2S03, doi:10.1029/2005RS003431.

Yee K (1966) Numerical solution of initial boundary value problems involving Maxwell's equations in isotropic media. IEEE Trans. Antennas Propagation 14:302-307.

Yu Y, Simpson J J (submitted) An E-J collocated 3-D FDTD model of electromagnetic wave propagation in magnetized cold plasma. IEEE Trans. Antennas Propagation.

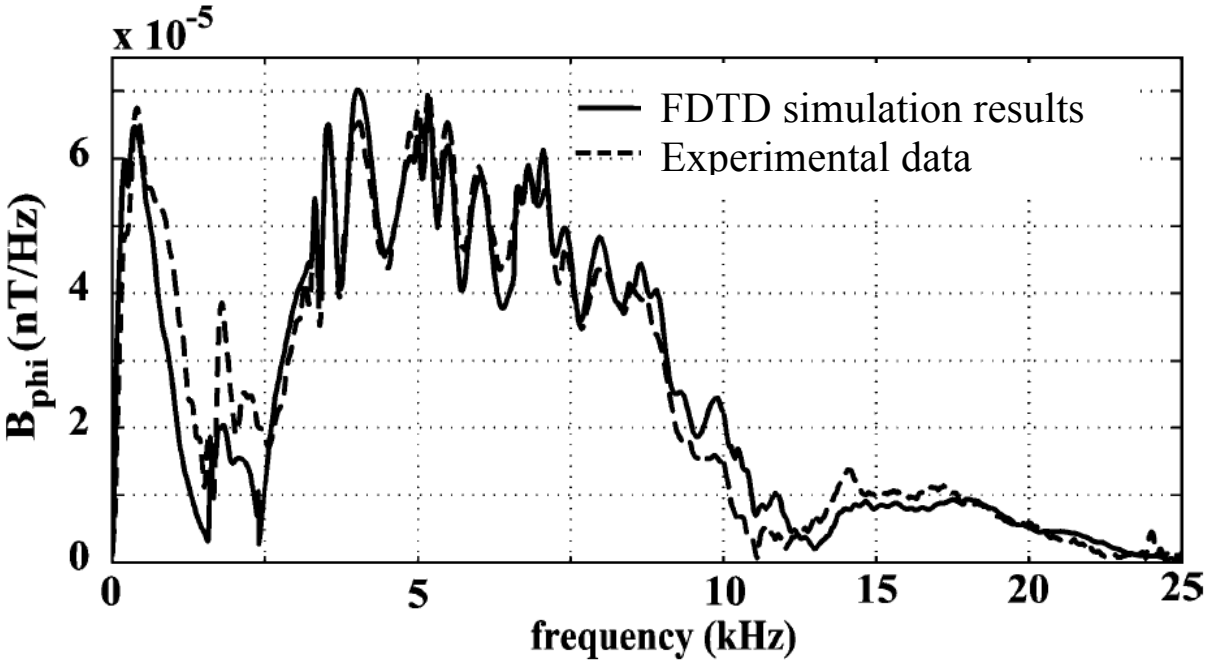

Fig. 1 Comparison up to 25 kHz between experimental data collected by a sensor at Duke University and the 2-D cylindrical FDTD-calculated predictions described in [Hu and Cummer 2006] (figure adapted from [Hu and Cummer 2006]).

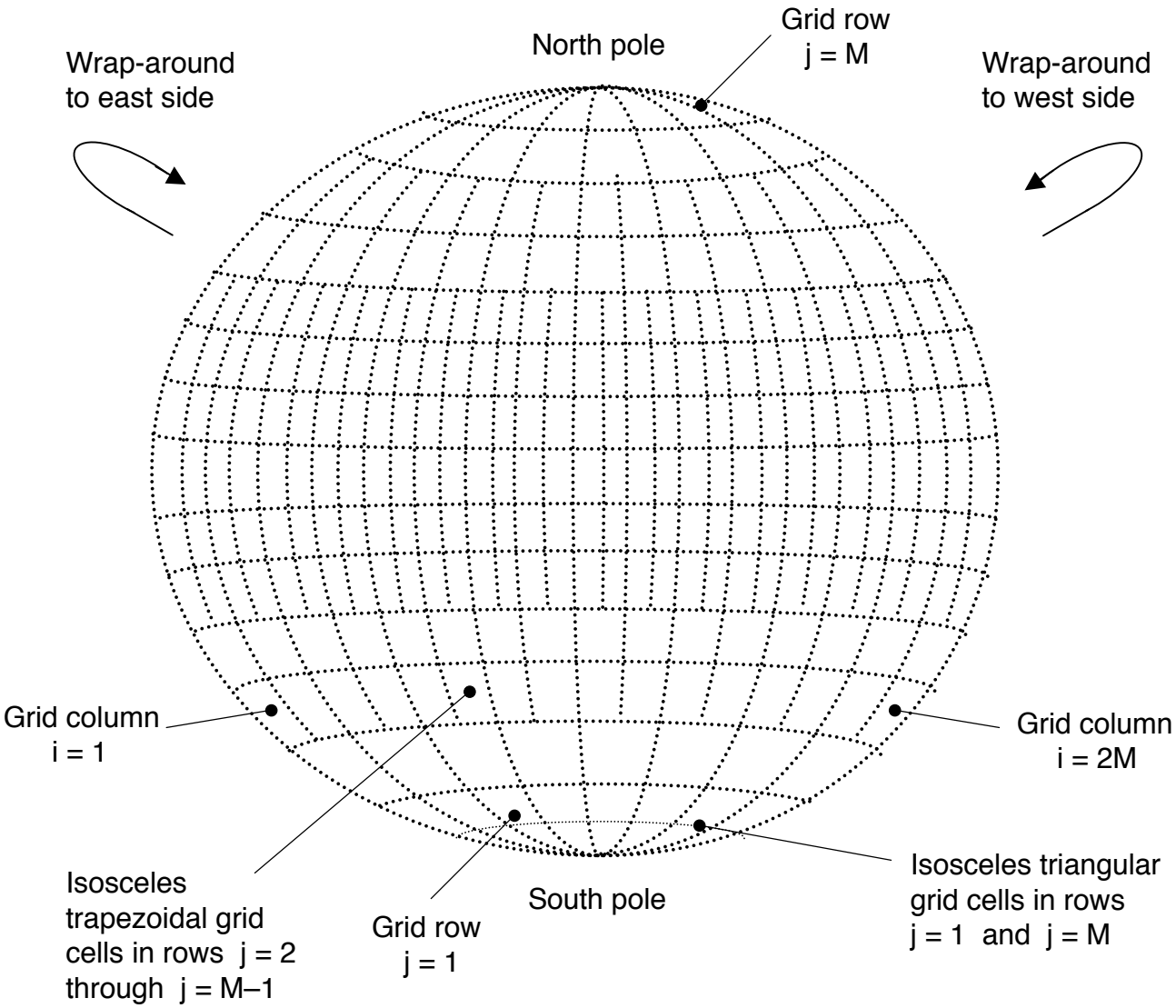

Fig. 2. General layout of the latitude-longitude FDTD Earth-ionosphere waveguide model as seen from a constant radial coordinate (Figure courtesy of [Simpson and Taflove 2002]).

UU IR Author Manuscript

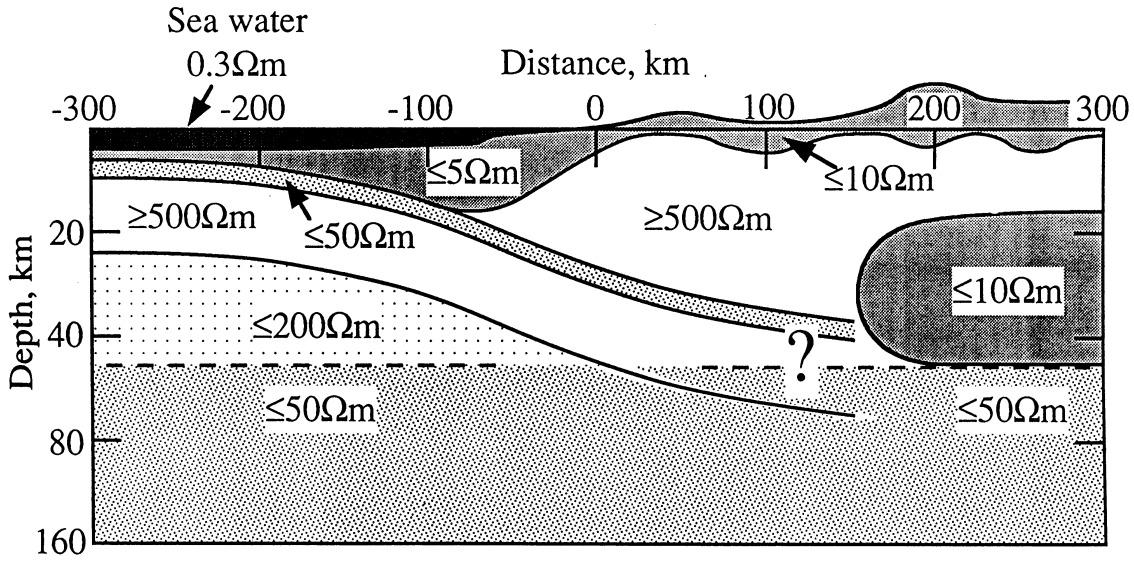

Fig. 3. Conductivity values used for the lithosphere in the 3-D global FDTD model of [Simpson and Taflove 2004a, Simpson et al. 2006] according to whether the space lattice point is located directly below an ocean or within a continent (figure courtesy of [Hermance 1995]).

UU IR Author Manuscript

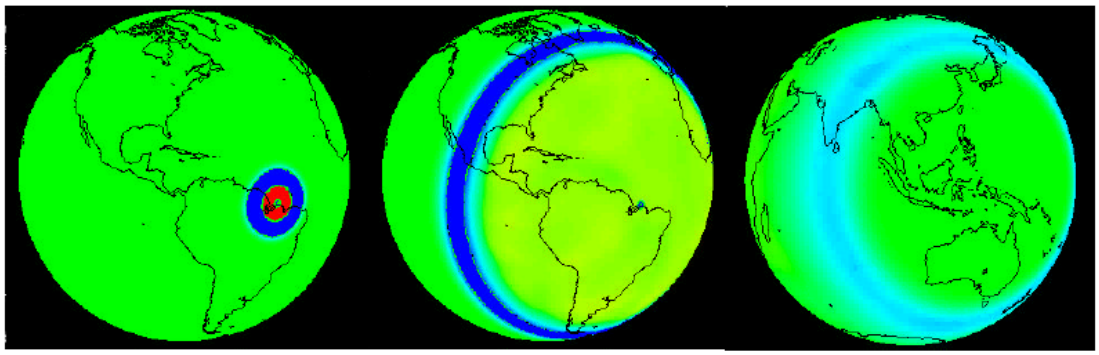

Fig. 4. Snapshots of impulsive wave propagation around the Earth as calculated by the 3-D FDTD model of [Simpson and Taflove 2004a] (the complete video can be downloaded at http://www.ece.unm.edu/~simpson/3Dmovietext@gif.avi) (figure courtesy of [Taflove and Simpson 2005]).

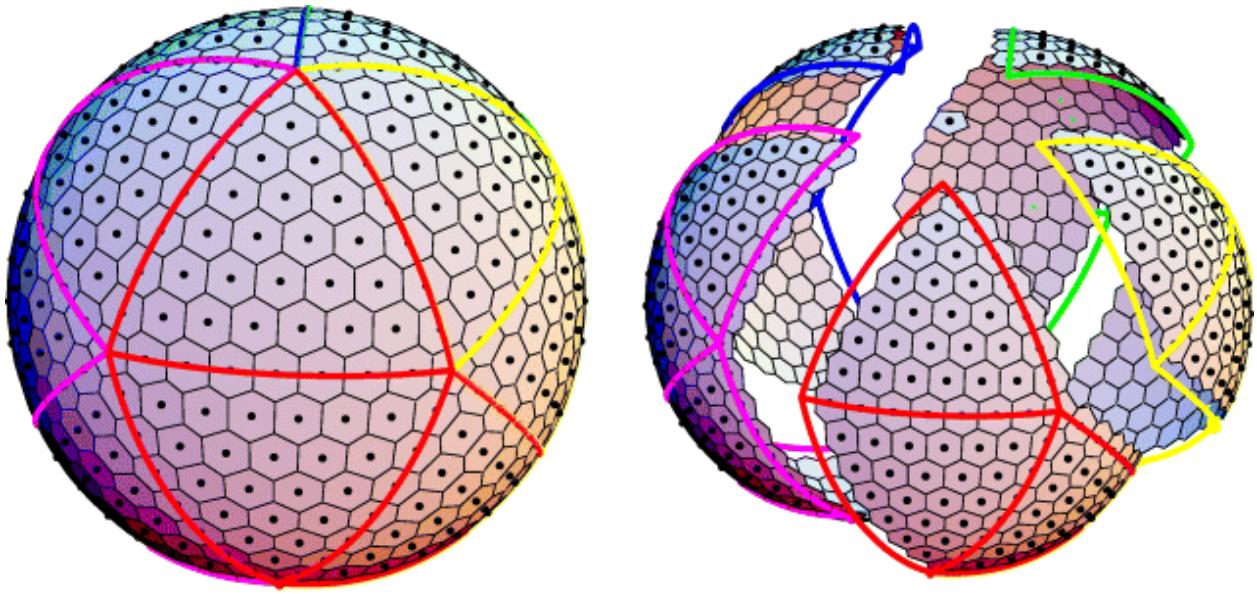

(a) (b)

Fig. 5. General layout of a sample 642-cell geodesic grid covering the complete Earth-sphere as seen from a constant radial coordinate (Figure courtesy [Randall et al. 2002]). This geometry layout is the basis for the 3-D FDTD geodesic Earth-ionosphere model of [Simpson et al. 2006].

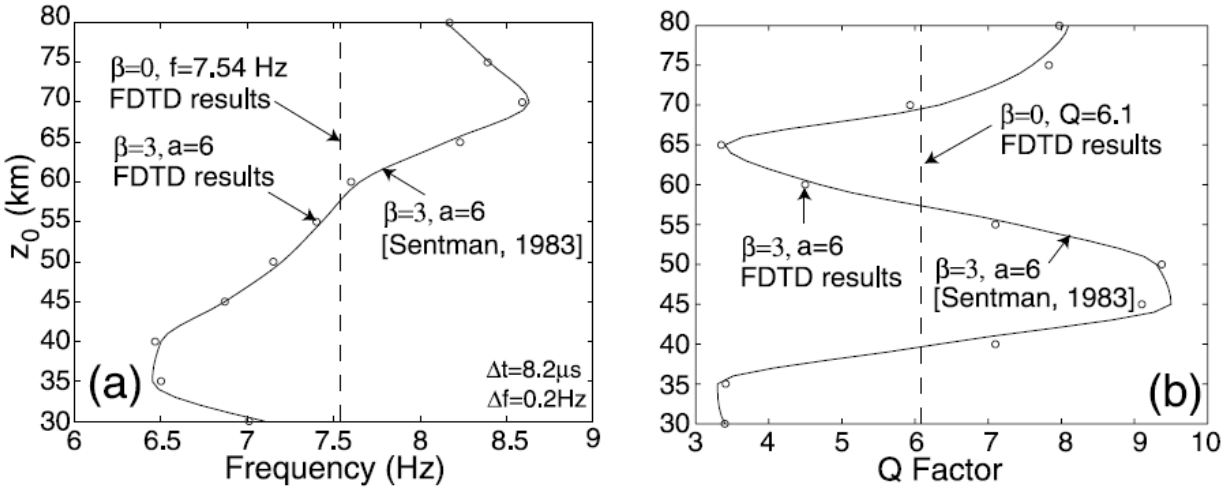

Fig. 6 Comparison between the analytical (mode theory) results of [Sentman 1983] and the 3-D FDTD-calculated results of [Yang and Pasko 2005] for the first Schumann resonance eigenfrequency (a) and Q-factor (b) as a function of the altitude (z_0) of the perturbation in the single-exponential ionosphere conductivity profile (figure courtesy of [Yang and Pasko 2005]). The parameter β is the amplitude of the perturbation in powers of ten about its unperturbed value, and "a" is the width of the perturbation.

UU IR Author Manuscript

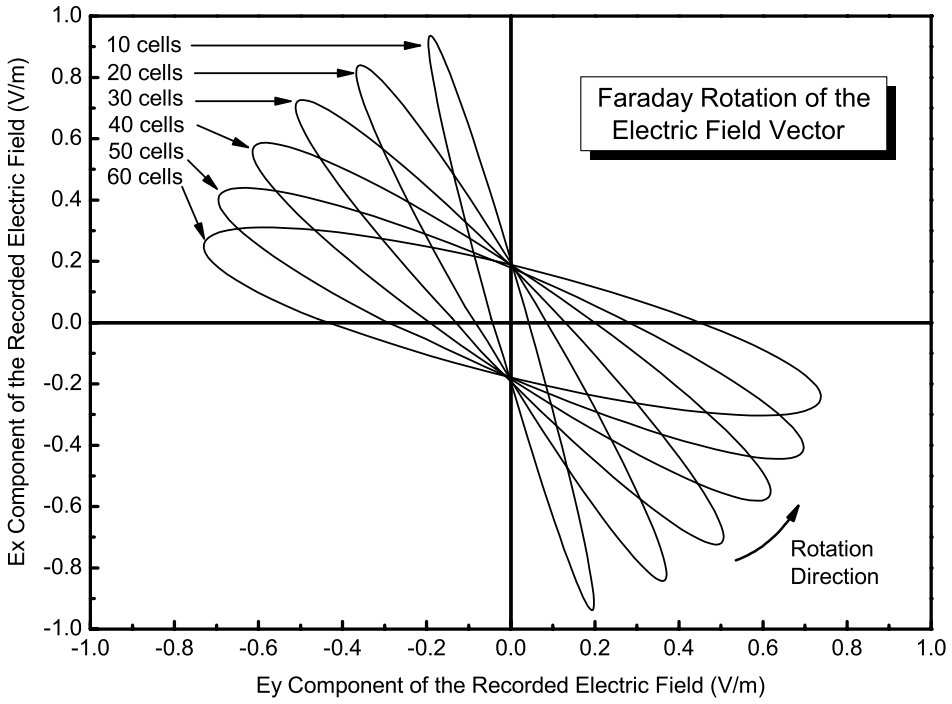

Fig. 7 Demonstration of the Faraday rotation effect in a 3-D Cartesian-coordinate FDTD model of magnetized cold plasma. (Figure courtesy of [Yu and Simpson, submitted]).

UU IR Author Manuscript